

Vertex renormalization in dc conductivity of doped chiral graphene

E. Cappelluti^{1,2} and L. Benfatto^{3,1,2}

¹SMC Research Center, CNR-INFN, and ISC-CNR, via dei Taurini 19, 00185 Roma, Italy

²Dipartimento di Fisica, Università “La Sapienza,” P. le A. Moro 2, 00185 Roma, Italy

³Centro Studi e Ricerche “Enrico Fermi,” via Panisperna 89/A, I-00184 Roma, Italy

(Received 29 September 2008; revised manuscript received 3 December 2008; published 29 January 2009)

The remarkable transport properties of graphene follow not only from the Dirac-type energy dispersion, but also from the chiral nature of its excitations, which makes unclear the limits of applicability of the standard semiclassical Boltzmann approach. In this paper we provide a quantum derivation of the transport scattering time in graphene in the case of electron-phonon interaction. By using the Kubo formalism, we compute explicitly the vertex corrections to the dc conductivity by retaining the full chiral matrix structure of graphene. We show that at least in the regime of large chemical potential the Boltzmann picture is justified. This result is also robust against a small sublattice inequivalence, which partly spoils the role of chirality and leads to a doping dependence of the resistivity that can be relevant to recent transport experiments in doped graphene samples.

DOI: [10.1103/PhysRevB.79.035419](https://doi.org/10.1103/PhysRevB.79.035419)

PACS number(s): 81.05.Uw, 72.10.Di, 63.20.kd

I. INTRODUCTION

The physical properties of doped and undoped graphene are the subject of an intense investigation in the view of possible applications of these materials in electronic and optical devices. A precise characterization of its transport and optical properties is thus a compelling issue. In addition to its relevance for technological applications, graphene poses several unusual and interesting theoretical problems. The low-energy properties are dominated by the Dirac-type excitations at the so-called K and K' points of the Brillouin zone, where the tight-binding electronic dispersion of the graphene honeycomb lattice can be approximated as $\epsilon_{\mathbf{k}} = \pm \hbar v_F |\mathbf{k}|$. Here \mathbf{k} is the relative momentum with respect to the K (K') point.¹ An additional ingredient is also the chiral character of the bands, which gives rise to the well-known absence of backward scattering in transport.² Note that, although obviously related in graphene, these two issues are formally distinct and are associated with different phenomenologies. A Dirac-type behavior can be induced, for instance, in nodal d -wave superconductors, as cuprates, without any relation to chirality.³⁻⁵ On the other hand a chiral structure is still present even in bilayer graphene, where the low-energy bands acquire a parabolic character.⁶

Transport properties represent a particular delicate issue in graphene. As in any other system, also for graphene the full quantum treatment of transport processes would require the explicit evaluation of the current vertex corrections for the conductivity.^{7,8} Indeed, only by going beyond the so-called bare-bubble approximation, one can recover the distinction between the transport relaxation time τ_{tr} and the “quasiparticle” one τ_{qp} (relevant, for instance, for photoemission measurements). However, the chiral nature of excitations in graphene increases considerably the complexity of this approach. For this reason, transport properties are often discussed in doped graphene (i.e., when the chemical potential is far from the Dirac point) within the framework of the semiclassical Boltzmann theory.⁹⁻¹⁷ In this context, τ_{tr} differs from τ_{qp} for a weighted average of the scattering probability

with the angular factor $(1 - \cos \theta)$ (where θ is the angle between incoming and outgoing scattering electrons). As usual, this leads to the suppression of *forward*-scattering processes.^{18,19}

Even though a general expectation holds that the Boltzmann theory should be valid for doped graphene, the application of this approach to a chiral system such as graphene is far from being trivial. Indeed, due to the multiband chiral structure, the velocity operator $\hat{v}_{\mathbf{k}} = \hbar^{-1} d\hat{H}_{\mathbf{k}}/d\mathbf{k}$ in graphene does not commute with the Hamiltonian $\hat{H}_{\mathbf{k}} = \hbar v_F \mathbf{k} \cdot \boldsymbol{\sigma}$ itself, where $\mathbf{k} = (k_x, k_y)$ and $\boldsymbol{\sigma} = (\hat{\sigma}_x, \hat{\sigma}_y)$ is the vector of the Pauli matrices. As it has been observed by many authors,²⁰⁻²² this fact poses several doubts on the applicability of conventional Boltzmann theory. In the Boltzmann theory indeed one assumes that the equilibrium distribution function $f(\epsilon_{\mathbf{k}})$ in the presence of the external electric field \mathbf{E} can be described in terms of the one in the absence of external fields as $f_{\mathbf{E}}(\mathbf{k}) \approx f^0(\epsilon_{\mathbf{k}} - e\tau_{tr}\mathbf{v}_{\mathbf{k}} \cdot \mathbf{E})$, where $\mathbf{v}_{\mathbf{k}} = \hbar^{-1} d\epsilon_{\mathbf{k}}/d\mathbf{k}$ and e is the electron charge.²³ An important underlying assumption here is that the energy eigenvalue $\epsilon_{\mathbf{k}}$ is a good quantum number as well as the shifted quantity $\epsilon_{\mathbf{k}} - e\tau_{tr}\mathbf{v}_{\mathbf{k}} \cdot \mathbf{E}$. This would imply that the energy Hamiltonian operator $\hat{H}_{\mathbf{k}}$ and the velocity operator $\hat{v}_{\mathbf{k}}$ commute so that they can be diagonalized *simultaneously*. As discussed above, however, this condition is not fulfilled in chiral graphene. To overcome this problem alternative approaches based on quantum and/or quasiclassical kinetic equations have been employed, where distribution functions and the corresponding density operators are defined in a chiral matrix space.^{20,22}

A second potential limit in the applicability of the Boltzmann theory concerns the origin of the angular factor $(1 - \cos \theta)$ in the expression of the transport scattering time. Indeed, in conventional systems it originates from the momentum dependence of the current operator $\hat{j}(\mathbf{k}) = (e/\hbar) d\hat{H}_{\mathbf{k}}/d\mathbf{k}$, which points along the \mathbf{k} direction in the isotropic case, $\hat{j}(\mathbf{k}) \propto \mathbf{k}/|\mathbf{k}|$. It is precisely such directional dependence which gives rise to the angular factor $1 - \mathbf{v}_{\mathbf{k}} \cdot \mathbf{v}_{\mathbf{k}'} / |\mathbf{v}_{\mathbf{k}}|^2 \approx 1 - \mathbf{k} \cdot \mathbf{k}' / |\mathbf{k}|^2 = 1 - \cos \theta$ in the transport

properties.^{7,8} Things are drastically different in the case of graphene, where we have

$$\hat{j}(\mathbf{k}) = \frac{e}{\hbar} \frac{d\hat{H}_{\mathbf{k}}}{d\mathbf{k}} = ev_F \boldsymbol{\sigma}.$$

The important feature to be stressed is that the bare vertex current operator is here \mathbf{k} independent; i.e., it does not depend on the direction of the momentum $\mathbf{k}=(k_x, k_y)$. Thus the possible relevance of the angular factor $(1-\cos\theta)$ suppressing forward scattering in the transport properties should be better assessed. This is particularly important when the scattering processes involve a momentum dependence more complex than the short-range impurity scattering discussed in Refs. 24–26. A typical example is provided by the scattering of electrons by acoustic phonons, which plays a major role in controlling the temperature dependence of the dc conductivity.^{27,28}

In order to assess these open issues, we provide in this paper an explicit derivation of the dc conductivity in doped graphene using a fully quantum approach for the electron-phonon (el-ph) scattering based on the Kubo formula. Indeed, in nonchiral systems this procedure is known to give a quantum derivation of the Boltzmann theory.^{7,8} In the case of graphene this program can be fulfilled only by retaining the full chiral structure in the explicit calculation of the current vertex corrections. In the limit where the chemical potential is larger than the quasiparticle scattering time, an analytical solution can be derived. We show that, in spite of the above argumentations, at least in this regime the results of the Boltzmann theory are still valid, in the sense that the forward-scattering suppression in the transport relaxation rate is still operative, as resulting from the additional angular factor $(1-\cos\theta)$ in τ_{tr} . This result follows from the fact that the dependence on the momentum angle of the vertex function is strictly replaced by a corresponding angular dependence in the pseudospin space, encoded in the Pauli matrix structure. We investigate the applicability of the Boltzmann results also in the presence of a weak inequivalence between the two carbon sublattices, which, close to the Dirac point, leads to a mixing of the chiral eigenstates.^{29,30} We show that even in this case the Boltzmann results are recovered. The present quantum approach provides in addition a basis for the future calculation of the quantum vertex corrections at finite frequency and in the Dirac limit, which can be both relevant for a direct comparison with existing experimental data.^{27,28,31}

The structure of the paper is the following. In Sec. II we introduce the Hilbert space we are working with and the basic formalism for the electron-phonon interaction, while in Sec. III we evaluate the self-energy due to the electron-phonon interaction in graphene. In Sec. IV we implement the calculation of the vertex corrections for the dc conductivity, and we derive the explicit expression for the transport scattering rate. In Sec. V we report the results in the presence of an additional weak inequivalence between the two sublattices, which breaks the chirality preserving the Boltzmann approach. In Sec. VI we discuss some possible observable effects of our analysis in relation to the doping dependence of the high-temperature linear slope of the resistivity, and in

Sec. VII we summarize our conclusions. In Appendixes A and B we include some details on the calculation of the Eliashberg functions and on the gapped case, respectively.

II. MODEL

In order to point out the relevance of the angular transport factor $(1-\cos\theta)$ in chiral doped graphene, we consider in this paper the effects of electron scattering with acoustic phonons. Let us start by introducing the general electron-phonon Hamiltonian in terms of the usual orbital spinor $\psi_{\mathbf{k}}^{\dagger}=(c_{\mathbf{k},A}^{\dagger}, c_{\mathbf{k},B}^{\dagger})$, where $c_{\mathbf{k},A}^{\dagger}$ and $c_{\mathbf{k},B}^{\dagger}$ represent the creation operators of one electron with momentum \mathbf{k} on sublattices A and B , respectively. In this basis we can write

$$\begin{aligned} \hat{H} = & N_s \sum_{\mathbf{k}} \psi_{\mathbf{k}}^{\dagger} \hat{H}_{\mathbf{k}}^0 \psi_{\mathbf{k}} + \sum_{\mathbf{q}, \nu} \omega_{\mathbf{q}, \nu} a_{\mathbf{q}, \nu}^{\dagger} a_{\mathbf{q}, \nu} \\ & + N_s \sum_{\mathbf{k}, \mathbf{q}, \nu} \psi_{\mathbf{k}+\mathbf{q}}^{\dagger} \hat{g}_{\mathbf{k}, \mathbf{k}+\mathbf{q}, \nu} \psi_{\mathbf{k}} (a_{\mathbf{q}, \nu} + a_{-\mathbf{q}, \nu}^{\dagger}). \end{aligned}$$

Here $\hat{H}_{\mathbf{k}}^0$ is the noninteracting tight-binding electron Hamiltonian,

$$\hat{H}_{\mathbf{k}}^0 = \begin{pmatrix} 0 & f^*(\mathbf{k}) \\ f(\mathbf{k}) & 0 \end{pmatrix}, \quad (1)$$

where $f^*(\mathbf{k})$ is the Fourier transform of the tight-binding model on the honeycomb lattice, $a_{\mathbf{q}, \nu}^{\dagger}$ is the creation operator of one phonon with momentum \mathbf{q} in the ν branch, $\omega_{\mathbf{q}, \nu}$ is the corresponding frequency, and $\hat{g}_{\mathbf{k}, \mathbf{k}+\mathbf{q}, \nu}$ is the electron-phonon matrix element which presents in general a nontrivial matrix structure. $N_s=2$ takes into account here the spin degeneracy which will play no role in the following.

In this paper we shall work in the original basis of electron operators for the A and B sublattices, as described in Eq. (1). This choice results to be more convenient in the evaluation of the transport properties from a linear-response theory based on the Kubo formula. As an alternative approach the eigenvector basis, in which Hamiltonian (1) is diagonal, was employed in Refs. 20–22 since it makes easier the implementation of a quantum or quasiclassical extension of the kinetic equations.

A compelling treatment of the electron-phonon interaction including the full phonon spectrum for all \mathbf{q} 's is a formidable task due to the complex matrix structure of the elements $\hat{g}_{\mathbf{k}, \mathbf{k}+\mathbf{q}, \nu}$. Fortunately, since in weakly doped graphene the electron momenta are close to the Dirac point, the relevant exchanged phonons are mainly located either close to the K, K' edge zone or at the Γ ($\mathbf{q}=0$) point. Detailed analysis of the electron-phonon effects for general acoustic and optical modes can be found in Refs. 32–39. We concentrate here on the electron-phonon scattering with the acoustic modes with $\mathbf{q} \approx 0$, which are dominant in the dc transport properties at low temperatures. Several simplifications can be employed in this case. First of all, the phonon dispersion can be simply linearized, $\omega_{\mathbf{q}, \nu} \approx \hbar v_s |\mathbf{q}|$. In addition for $\mathbf{q} \rightarrow 0$ the charge modulation wavelength $\lambda=1/|\mathbf{q}|$ is much larger than the interatomic distance a . In this regime the two carbon atoms of the unitary cell are essentially indistinguishable so that the

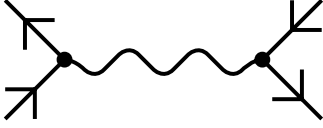


FIG. 1. Diagrammatic representation of the electron-phonon interaction. Straight lines represent incoming and outgoing electrons, the wavy line is the phonon propagator, and the filled circles are the el-ph matrix elements.

electron-phonon matrix element behaves as $\hat{g}_{\mathbf{k},\mathbf{k}+\mathbf{q}} \approx g_{\mathbf{k},\mathbf{k}+\mathbf{q}} \hat{I}$ in the chiral space. Within the same assumption, we can also neglect intervalley scattering and discuss interactions within a single Dirac cone.²⁴ Finally, for small doping, we can linearize the electron dispersion close to the Dirac points, $\hat{H}_{\mathbf{k}}^0 = \hbar v_F \mathbf{k} \cdot \boldsymbol{\sigma}$. We can write thus our effective Hamiltonian as

$$\begin{aligned} \hat{H} = & N_s N_k \sum_{\mathbf{k}} \psi_{\mathbf{k}}^\dagger \hbar v_F \mathbf{k} \cdot \boldsymbol{\sigma} \psi_{\mathbf{k}} + \sum_{\mathbf{q}} \hbar v_s |\mathbf{q}| a_{\mathbf{q}}^\dagger a_{\mathbf{q}} \\ & + N_s N_K \sum_{\mathbf{k},\mathbf{q}} g_{\mathbf{q}} \psi_{\mathbf{k}+\mathbf{q}}^\dagger \hat{I} \psi_{\mathbf{k}} (a_{\mathbf{q}} + a_{-\mathbf{q}}^\dagger), \end{aligned} \quad (2)$$

where we made use of the relation $g_{\mathbf{k},\mathbf{k}+\mathbf{q}} \approx g_{\mathbf{q}}$ for $\mathbf{q} \rightarrow 0$.

The resulting electron-phonon coupling is usually expressed in terms of the kernel $W_{\mathbf{k}-\mathbf{k}'}(\omega-\omega')$, which is diagrammatically depicted in Fig. 1 and which represents the effective retarded interaction between two electrons with momenta \mathbf{k} and \mathbf{k}' and energies ω and ω' , which exchange momentum $\mathbf{k}-\mathbf{k}'$ and energy $\omega-\omega'$. From Eq. (2) we have

$$W_{\mathbf{k}-\mathbf{k}'}(\omega-\omega') = |g_{\mathbf{k}-\mathbf{k}'}|^2 D_{\mathbf{k}-\mathbf{k}'}(\omega-\omega'), \quad (3)$$

where $D_{\mathbf{q}}(\Omega) = 2\omega_{\mathbf{q}} / [\omega_{\mathbf{q}}^2 - \Omega^2]$ is the phonon propagator. Note that, since $\hat{g}_{\mathbf{q}} \propto \hat{I}$ in the limit $\mathbf{q} \rightarrow 0$, Eq. (3) does not present a matrix structure, simplifying notably the calculations. It is also convenient to express the effective retarded interaction in terms of the Eliashberg function $\alpha^2 F(\mathbf{q}, \Omega)$:

$$W_{\mathbf{k}-\mathbf{k}'}(\omega-\omega') = \int d\Omega \frac{2\Omega \alpha^2 F(\mathbf{k}-\mathbf{k}', \Omega)}{\Omega^2 - (\omega-\omega')^2}, \quad (4)$$

where $\alpha^2 F(\mathbf{k}-\mathbf{k}', \Omega) = |g_{\mathbf{k}-\mathbf{k}'}|^2 \delta(\Omega - \omega_{\mathbf{k}-\mathbf{k}'})$.

In this paper we shall focus on the case of intrinsically doped graphene, where the chemical potential $|\mu|$ is much larger than both the allowed exchanged phonon energies ω_{\max} and the quasiparticle scattering rate Γ_{qp} . Note that in the case of acoustic phonons, the highest exchanged phonon energy ω_{\max} is given by the Bloch-Grüneisen energy scale $\omega_{\max} = 2\hbar v_s k_F$, so that the constraint $|\mu| \gg \omega_{\max}$ implies $v_F \gg v_s$, which is always fulfilled in graphene. The condition $\Gamma_{\text{qp}} \ll |\mu|$, on the other hand, is doping dependent and it is usually fulfilled in doped graphene. In this situation, since electrons are scattered only within a narrow energy window $\pm \omega_{\max}$ around the Fermi level, we can put the electron momenta appearing in the Eliashberg function on the Fermi surface, so that it depends only on the relative angle. Writing $\mathbf{k} = k(\cos \phi, \sin \phi)$ (see Fig. 2), we have thus $k \approx k' \approx k_F$, and we can write $|\mathbf{q}| = 2k_F \sin[(\phi - \phi')/2]$ and $\alpha^2 F(\mathbf{k}-\mathbf{k}', \Omega) = \alpha^2 F(\phi - \phi', \Omega)$. Moreover, the condition $|\mu| \gg \omega_{\max}, \Gamma_{\text{qp}}$ allows us also to restrict ourselves to a single electron (hole)

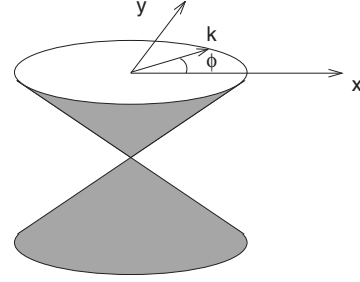


FIG. 2. Sketch of the cylindrical coordinates used in the paper. In this coordinate basis we can write $\mathbf{k} = k(\cos \phi, \sin \phi)$.

cone for $\mu > 0$ ($\mu < 0$), with a significant simplification of the calculations [see Eq. (18) below].

Before discussing the one-particle self-energy, let us briefly summarize the properties of the noninteracting system whose Green's function per spin and valley, in the Matsubara space, reads

$$\begin{aligned} \hat{G}^0(\mathbf{k}, i\omega_n) &= \frac{1}{(i\hbar\omega_n + \mu)\hat{I} - \hbar v_F \mathbf{k} \cdot \boldsymbol{\sigma}} \\ &= \frac{(i\hbar\omega_n + \mu)\hat{I} + \hbar v_F \mathbf{k} \cdot \boldsymbol{\sigma}}{[(i\hbar\omega_n + \mu)^2 - (\hbar v_F k)^2]}. \end{aligned} \quad (5)$$

We can expand the Green's function in the Pauli matrix basis,

$$\hat{G}^0(\mathbf{k}, i\omega_n) = \sum_{i=x,y} G_i^0(\mathbf{k}, i\omega_n) \hat{\sigma}_i. \quad (6)$$

It is easy to see, from Eqs. (5) and (6), that the diagonal part $G_x^0(\mathbf{k}, i\omega_n)$ depends only on the $\epsilon = \hbar v_F k$ ($k = |\mathbf{k}|$), while the off-diagonal components depend also on the angle ϕ . In particular, we can write explicitly

$$G_x^0(\mathbf{k}, i\omega_n) = G_+^0(\epsilon, i\omega_n),$$

$$G_x^0(\mathbf{k}, i\omega_n) = G_-^0(\epsilon, i\omega_n) \cos \phi,$$

$$G_y^0(\mathbf{k}, i\omega_n) = G_-^0(\epsilon, i\omega_n) \sin \phi,$$

where

$$G_{\pm}^0(\epsilon, i\omega_n) = \frac{1}{2} \left[\frac{1}{i\hbar\omega_n + \mu - \epsilon} \pm \frac{1}{i\hbar\omega_n + \mu + \epsilon} \right].$$

III. ONE-PARTICLE SELF-ENERGY

Let us now consider the one-particle self-energy for the electron-phonon interaction. As mentioned, we are interested here in the limit $|\mu| \gg \omega_{\max}$. In this regime the theorem of Migdal⁴⁰ assures the validity of the standard mean-field-like theory of Eliashberg.⁴¹ The corresponding self-energy is thus diagrammatically depicted in Fig. 3, and it can be written in Matsubara space as

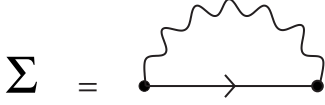


FIG. 3. Diagrammatic representation of the electron-phonon self-energy. Graphical elements as in Fig. 1.

$$\hat{\Sigma}(\mathbf{k}, n) = T \sum_{\mathbf{k}', m} W_{\mathbf{k}-\mathbf{k}'}(n-m) \hat{G}(\mathbf{k}', m), \quad (7)$$

where $\hat{G}(\mathbf{k}, n) = \hat{G}(\mathbf{k}, i\omega_n)$, $\hat{\Sigma}(\mathbf{k}, n) = \hat{\Sigma}(\mathbf{k}, i\omega_n)$, and $W_{\mathbf{k}-\mathbf{k}'}(n-m) = W_{\mathbf{k}-\mathbf{k}'}(i\omega_n - i\omega_m)$.

From the Dyson equation we can write

$$\hat{G}(\mathbf{k}, n) = \frac{1}{(i\hbar\omega_n + \mu) \hat{I} - \hbar v_F \mathbf{k} \cdot \boldsymbol{\sigma} - \hat{\Sigma}(\mathbf{k}, n)}.$$

Since Eq. (7) is a convolution both in momentum and frequency space, it is easy to show that the matrix self-energy admits the analogous decomposition (6) of Green's function (6), namely,

$$\hat{\Sigma}(\mathbf{k}, n) = \sum_{i=L,x,y} \Sigma_i(\mathbf{k}, n) \hat{\sigma}_i,$$

where $\Sigma_I(\mathbf{k}, n) = \Sigma_I(\epsilon, n)$, $\Sigma_x(\mathbf{k}, n) = \Sigma_x(\epsilon, \phi, n) = \Sigma_{\text{off}}(\epsilon, n) \cos \phi$, and $\Sigma_y(\mathbf{k}, n) = \Sigma_y(\epsilon, \phi, n) = \Sigma_{\text{off}}(\epsilon, n) \sin \phi$, where the label ‘‘off’’ characterizes the *off*-diagonal elements of the self-energy.

Using the Dyson equation, we can write once more $G_I(\mathbf{k}, n) = G_+(k, n)$, $G_x(\mathbf{k}, n) = G_-(\epsilon, n) \cos \phi$, and $G_y(\mathbf{k}, n) = G_-(\epsilon, n) \sin \phi$, with

$$G_{\pm}(\epsilon, n) = \frac{1}{2} \left[\frac{1}{i\hbar\omega_n + \mu - \epsilon - \Sigma_I(\epsilon, n) - \Sigma_{\text{off}}(\epsilon, n)} \pm \frac{1}{i\hbar\omega_n + \mu + \epsilon - \Sigma_I(\epsilon, n) + \Sigma_{\text{off}}(\epsilon, n)} \right]. \quad (8)$$

The calculation of Eq. (7) is straightforward in the case of intrinsically doped graphene. As discussed above, the relevant electron momenta are here restricted on the Fermi surface, $\mathbf{k} \approx k_F$ ($\epsilon = \mu$), so that self-energy (7) depends only on the angular part of the \mathbf{k} vector, $\Sigma_i(\epsilon, \phi, n) \approx \Sigma_i(\phi, n)$. We can also split the sum over \mathbf{k}' in Eq. (7) in its energy and angular degrees of freedom, $\Sigma_{\mathbf{k}} \rightarrow \int_{-\pi}^{\pi} d\phi / 2\pi \int_0^W d\epsilon N(\epsilon)$, where W is the electron bandwidth, and $N(\epsilon) = \epsilon V / 2\pi \hbar^2 v_F^2$ is the density of states per spin and per valley, and V is the unit-cell volume. Thus we have

$$\Sigma_i(\phi, n) = T \sum_m \int \frac{d\phi'}{2\pi} W_{\phi-\phi'}(n-m) \chi_i(\phi') G_{i,\text{loc}}(m), \quad (9)$$

where $\chi_I = 1$, $\chi_x(\phi) = \cos \phi$, $\chi_y(\phi) = \sin \phi$, and $G_{i,\text{loc}}(m)$ is the local (\mathbf{k} -averaged) Green's function: $G_{I,\text{loc}}(m) = G_{+,\text{loc}}(m) = \int N(\epsilon) d\epsilon G_+(\epsilon, m)$ and $G_{x,y,\text{loc}}(m) = G_{-,\text{loc}}(m) = \int N(\epsilon) d\epsilon G_-(\epsilon, m)$.

It is useful at this stage to introduce the basis of the two-dimensional spherical harmonics

$$\psi_{\alpha}(\phi) = e^{i\alpha\phi}, \quad \alpha = 0, \pm 1, \pm 2, \dots,$$

so that we can decompose any generic angle-dependent function $S(\phi)$ on this basis,

$$S(\phi) = \sum_{\alpha} S_{\alpha} \psi_{\alpha}(\phi), \quad (10)$$

where

$$S_{\alpha} = \int \frac{d\theta}{2\pi} S(\theta) \psi_{\alpha}^*(\theta). \quad (11)$$

Using definition (4) of the electron-phonon kernel, we can write the diagonal and off-diagonal components of the self-energy in Eq. (9) as

$$\Sigma_I(n) = T \sum_m \int d\Omega \frac{2\Omega \alpha^2 F_0(\Omega)}{\Omega^2 + (\omega_n - \omega_m)^2} G_{+,\text{loc}}(m), \quad (12)$$

$$\Sigma_{\text{off}}(n) = T \sum_m \int d\Omega \frac{2\Omega \alpha^2 F_1(\Omega)}{\Omega^2 + (\omega_n - \omega_m)^2} G_{-,\text{loc}}(m), \quad (13)$$

where $\alpha^2 F_{\alpha}$ are the projections of the Eliashberg function $\alpha^2 F(\phi)$ on the spherical harmonics $\psi_{\alpha}(\phi)$, according to decomposition (10) above.

Equations (12) and (13) can be easily analytically continued on the real-frequency axis using standard techniques. Through the imaginary part of the self-energy, we can thus define a *diagonal* and an *off-diagonal* scattering rate, $\Gamma_{I(\text{off})} = -\lim_{\omega \rightarrow 0} \text{Im} \Sigma_{I(\text{off})}(\omega + i0^+)$, where

$$\Gamma_I = -2\pi N(\mu) \int d\Omega \alpha^2 F_0(\Omega) [n(\beta\Omega) + f(\beta\Omega)] \times \text{Im}[G_{+,\text{loc}}(\Omega + i0^+)], \quad (14)$$

and where

$$\Gamma_{\text{off}} = -2\pi N(\mu) \int d\Omega \alpha^2 F_1(\Omega) [n(\beta\Omega) + f(\beta\Omega)] \times \text{Im}[G_{-,\text{loc}}(\Omega + i0^+)], \quad (15)$$

and where $n(x) = 1/[e^x - 1]$ and $f(x) = 1/[e^x + 1]$ are the Bose and Fermi factors, respectively.

For a practical evaluation of the self-energy terms, we can make use once more of the fact that, due to the low-energy phonon-mediated scattering, the relevant electron energies are restricted to the Fermi level. In this case we can write $\int_0^W d\epsilon N(\epsilon) \approx N(\mu) \int_0^W d\epsilon$ and, assuming $\mu > 0$, it is easy to see that only the upper Dirac cone [first term in Eq. (8)] is relevant. We have in particular $G_{+,\text{loc}}(\Omega + i0^+) \approx G_{-,\text{loc}}(\Omega + i0^+) = -i\pi N(\mu)/2$, so that, just as in common metals, the real part of the self-energy vanishes, and we have $\Gamma_I = 2K_0$ and $\Gamma_{\text{off}} = 2K_1$, where

$$K_{\alpha} = \frac{\pi N(\mu)}{2} \int d\Omega \alpha^2 F_{\alpha}(\Omega) [n(\beta\Omega) + f(\beta\Omega)]. \quad (16)$$

For the states at the Fermi energy, which involve only the upper band ($\mu > 0$), we can define thus a total quasiparticle scattering rate as

$$\Gamma_{\text{qp}} = \Gamma_I + \Gamma_{\text{off}} = 2K_0 + 2K_1, \quad (17)$$

which, using Eq. (8), gives the dressed Green's functions:

$$G_+(\epsilon, \omega) \approx G_-(\epsilon, \omega) \approx \frac{1}{2\hbar\omega + \mu - \epsilon + i\Gamma_{\text{qp}}}. \quad (18)$$

From Eqs. (14)–(17) we obtain finally

$$\begin{aligned} \Gamma_{\text{qp}} &= \pi N(\mu) \sum_{i=0,1} \int d\Omega \alpha^2 F_i(\Omega) [n(\beta\Omega) + f(\beta\Omega)] \\ &= \pi N(\mu) \int \frac{d\theta}{2\pi} g_\theta^2 (1 + \cos \theta) [n(\beta\omega_\theta) + f(\beta\omega_\theta)], \end{aligned} \quad (19)$$

where $g_\theta^2 = I|\mathbf{q}| = I2k_F \sin(\theta/2)$ and $\omega_\theta = \hbar v_s |\mathbf{q}| = 2\hbar v_s k_F \sin(\theta/2)$. Using the explicit expression for the K_α coefficients (see Appendix A), we obtain standard results with a $\Gamma_{\text{qp}} = [\pi^2 N(\mu) I / \hbar \omega_{\text{max}} v_s] T^2$ in the Bloch-Grüneisen regime ($T \lesssim \omega_{\text{max}}$) and $\Gamma_{\text{qp}} = [\pi N(\mu) I / \hbar v_s] T$ in the high-temperature $T \gtrsim \omega_{\text{max}}$ regime.

It is important to note that the total quasiparticle scattering rate arises from both the diagonal and off-diagonal contributions of the self-energy. Indeed, the explicit angular dependence shown in the second line of Eq. (19) points out that the off-diagonal terms, giving rise to the $\cos \theta$, are fundamental in order to recover the usual $(1 + \cos \theta)$ factor, which accounts for the well-known absence of backscattering in graphene due to chirality.^{14,18,19}

IV. DC CONDUCTIVITY

We implement now a full quantum treatment to evaluate the dc conductivity σ in the presence of vertex current renormalization. We consider thus the current-current response function^{7,8}

$$\begin{aligned} \Pi(m) &= \frac{N_s N_K}{V} T \sum_{\mathbf{k}, n} \text{Tr} [\hat{j}(\mathbf{k}) \hat{G}(\mathbf{k}, n) \\ &\quad \times \hat{J}(\mathbf{k}; n, n+m) \hat{G}(\mathbf{k}, n+m)], \end{aligned} \quad (20)$$

where $N_s, N_K = 2$ are the spin and valley degeneracies, respectively, $j(\mathbf{k}) = ev_F \hat{\sigma}_x$ is the bare current operator along the x axis, and $\hat{J}(\mathbf{k}; n, n+m)$ is the fully renormalized vertex current. The diagrammatic representation of the current-current response function is shown in Fig. 4. The dc conductivity will be obtained as the limit $\sigma = -\lim_{\omega \rightarrow 0} \text{Im} \Pi(\omega + i0^+) / \omega$ after the analytical continuation of the current-current response function Π on the real-frequency axis.

It is useful to remark here the importance in transport properties of the current-renormalization processes which account for the backflow cloud associated to the current of the quasiparticles. As discussed in Sec. I, one of the main effects of such current renormalization in normal metals is to give rise to the angular factor $(1 - \cos \theta)$ which differentiates the transport scattering rate Γ_{tr} from the quasiparticle one Γ_{qp} . We can understand this result by noting that in normal (isotropic) metals, the bare and the renormalized currents \mathbf{j} and

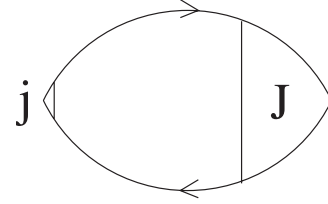


FIG. 4. Diagrammatic representation of the current-current response function Π . The small empty triangle on the left represents the bare current vertex $\hat{j}(\mathbf{k})$, while the big triangle on the right is the renormalized current vertex function $\hat{J}(\mathbf{k}; n, n+m)$.

\mathbf{J} , respectively, are both proportional to the velocity; i.e., they point in the direction of the momentum \mathbf{k} . Thus, one can write $\mathbf{J} = \Lambda \mathbf{k}$, where the vertex function Λ can be computed, for instance, in the ladder approximation. The self-consistent solution gives thus⁸

$$\langle \Gamma_{\text{tr}} \rangle_\theta \simeq \left\langle \Gamma_{\text{qp}} \left(1 - \frac{\mathbf{k} \cdot \mathbf{k}'}{k^2} \right) \right\rangle_\theta, \quad (21)$$

where \mathbf{k}, \mathbf{k}' are the momenta of the scattered electrons, with modulus equal to k_F but different directions, and $\langle \dots \rangle_\theta$ indicates the angular integration. This leads to the usual additional factor $(1 - \mathbf{k} \cdot \mathbf{k}' / k^2) = (1 - \cos \theta)$ in the angular average of the transport scattering time, which reproduces by means of a full quantum treatment the well-known semiclassical Boltzmann result.

While deriving result (21), a crucial ingredient is the proportionality between \mathbf{J} and the momentum \mathbf{k} . In graphene, where the energy-momentum dispersion is linear, such a relation clearly does not hold. However, as it is evident already at the level of the bare current \hat{j} , the matrix structure plays the analogous role of the momentum dependence in ordinary metals, so that \hat{j}_x , for example, is a matrix proportional to $\hat{\sigma}_x$. As far as the renormalized current is concerned, the analog of the momentum dependence in the ordinary metals becomes now a decomposition of \hat{J} in the Pauli matrices' components, by means of dimensionless function $\hat{\Lambda}$ defined by the relation $\hat{J}(\mathbf{k}; n, n+m) = ev_F \hat{\Lambda}(\mathbf{k}; n, n+m)$. As we shall see in what follows, in graphene such a matrix structure compensates—in a nontrivial way—for the lack of momentum dependence of the Fermi velocity, and leads once more to the Boltzmann result.

Aiming on focusing on the matricial structure of the current function, in the following we shall make use for the quantity of the same approximations employed for the self-energy. In particular, taking into account that the electron-phonon interaction gives rise only to low-energy scattering, we can approximate $\mathbf{k} \simeq k_F$ in the vertex function and retain only the angular dependence. In addition, one can decompose the vertex function in the basis of the Pauli matrices,

$$\hat{\Lambda}(\phi; n, n+m) = \sum_i \Lambda_i(\phi; n, n+m) \hat{\sigma}_i, \quad (22)$$

and we can expand the $\Lambda_i(\phi)$ functions in terms of the spherical harmonics components as in Eq. (10): $\Lambda_i(\phi; n,$

$n+m) = \sum_{\alpha} \Lambda_i^{\alpha}(n, n+m) \psi_{\alpha}(\phi)$. Inserting Eq. (22) into Eq. (20) and assuming, once more, for doped graphene that $G_+ \approx G_-$ (neglect of interband scattering), we obtain thus the general structure

$$\Pi(m) = \frac{2e^2 v_F^2 N_K N_S}{V} T \sum_n \Lambda^{\text{tot}}(n, n+m) b(n, n+m), \quad (23)$$

where $b(n, n+m) = N(\mu) \int d\epsilon G(\epsilon, n) G(\epsilon, n+m)$ (since $G_+ = G_-$ we have further dropped the index “ \pm ”) and where $\Lambda^{\text{tot}}(n, n+m) = \sum_{i,\alpha} c_i^{\alpha} \Lambda_i^{\alpha}(n, n+m)$. The c_i^{α} are numerical coefficients which arise from the angular average over ϕ . Since in bubble (20) one has the product of two Green’s functions, it is easy to realize that the angular average will involve at most harmonics up to the second order. Indeed, an explicit calculation shows that the only nonvanishing terms are

$$c_x^0 = c_l^1 = c_l^{-1} = 1, \quad (24)$$

$$c_x^2 = c_x^{-2} = -ic_y^2 = ic_y^{-2} = \frac{1}{2}. \quad (25)$$

Once the analytical continuation $i\omega_m \rightarrow \omega + i0^+$ of bubble (23) is performed and the limit $\omega \rightarrow 0$ is evaluated to compute the dc conductivity, one can see⁸ that only the advanced-retarded parts of the vertex function and of the b function contribute, so that

$$\sigma \simeq \frac{N_K N_S \hbar e^2 v_F^2}{\pi V} b_{\text{RA}}(0) \Lambda_{\text{RA}}^{\text{tot}}(0), \quad (26)$$

where $b_{\text{RA}}(\epsilon) = \lim_{\omega \rightarrow 0} b(\omega + i0^+, \omega - i0^+)$, and $\Lambda_{\text{RA}}^{\text{tot}}(0) = \lim_{\omega \rightarrow 0} \Lambda^{\text{tot}}(\omega + i0^+, \omega - i0^+)$. From Eq. (18) one easily finds

$$b_{\text{RA}}(0) = \frac{N(\mu)\pi}{4\Gamma_{\text{qp}}},$$

which gives the general expression for the dc conductivity in the presence of vertex corrections:

$$\sigma = \frac{N_K N_S \hbar e^2 v_F^2 N(\mu)}{4V\Gamma_{\text{tr}}}, \quad (27)$$

where we define the *transport* scattering rate

$$\Gamma_{\text{tr}} = \frac{\Gamma_{\text{qp}}}{\Lambda_{\text{RA}}^{\text{tot}}(0)}. \quad (28)$$

In the absence of vertex corrections [$\Lambda_{\text{RA}}^{\text{tot}}(0) = 1$] one recognizes in Eq. (27), as mentioned above in the case of ordinary metals, the standard result of the conductivity in the bare-bubble approximation,^{24,42} where the scattering time for transport coincides with the quasiparticle scattering time $\sigma = e^2 \mu / (2\pi \hbar \Gamma_{\text{qp}})$.

To compute Eq. (26) we need then to calculate the vertex corrections. In the doped-graphene regime we are interested in, this aim is made easy once more by the Migdal theorem which enforces the validity of the mean-field theory. The corresponding vertex function $\hat{\Lambda}(\mathbf{k}; n, n+m)$ can be evaluated thus within the self-consistent ladder approximation (see Fig. 5), namely,⁸



FIG. 5. Diagrammatic representation of the current vertex function. Graphical elements as in Fig. 1. The ladder approximation is enforced by the Migdal theorem valid for $|\mu| \gg \omega_{\text{max}}$.

$$\begin{aligned} \hat{\Lambda}(\mathbf{k}; n, n+m) &= \hat{\sigma}_x + T \sum_{\mathbf{k}', l} W_{\mathbf{k}-\mathbf{k}'}(n-l) \hat{G}(\mathbf{k}', l) \\ &\quad \times \hat{\Lambda}(\mathbf{k}'; l, l+m) \hat{G}(\mathbf{k}', l+m). \end{aligned} \quad (29)$$

In the same limit $|\mu| \gg \omega_{\text{max}}$, we can also employ the approximations implemented for the self-energy, namely, $|\mathbf{k}| \approx |\mathbf{k}'| \approx k_F$ and $\sum_{\mathbf{k}'} \rightarrow N(\mu) \int_{-\pi}^{\pi} d\phi' / 2\pi \int_{-\infty}^{\infty} d\epsilon'$, and we can also set $\hat{\Lambda}(\mathbf{k}'_F; l, l+m) = \hat{\Lambda}(\phi'; l, l+m)$ on the right-hand side of Eq. (29). Expanding again the $\hat{\Lambda}(\phi'; l, l+m)$ in terms of the Pauli basis and of the spherical harmonics, we end up with the following set of equations:

$$\begin{aligned} \Lambda_x^{\alpha}(n, n+m) &= \delta_{\alpha,0} + T \sum_{l,j,\beta} c_j^{\beta} W_{\alpha}(n-l) \\ &\quad \times b(l, l+m) \Lambda_j^{\beta+\alpha}(l, l+m), \end{aligned} \quad (30)$$

$$\Lambda_l^{\alpha}(n, n+m) = T \sum_{l,j,\beta} d_j^{\beta} W_{\alpha}(n-l) b(l, l+m) \Lambda_j^{\beta+\alpha}(l, l+m), \quad (31)$$

$$\Lambda_y^{\alpha}(n, n+m) = T \sum_{l,j,\beta} f_j^{\beta} W_{\alpha}(n-l) b(l, l+m) \Lambda_j^{\beta+\alpha}(l, l+m), \quad (32)$$

where the coefficients c_i^{α} are defined in Eqs. (24) and (25), and the only nonzero terms of the coefficients d_i^{α} and f_i^{α} are

$$d_l^0 = 2,$$

$$d_x^1 = d_x^{-1} = -id_y^1 = id_y^{-1} = 1,$$

$$f_y^0 = -if_l^1 = if_l^{-1} = 1,$$

$$-if_x^2 = if_x^{-2} = -f_y^2 = -f_y^{-2} = \frac{1}{2}.$$

We consider now the analytical continuation of Eqs. (30)–(32) on the real axis. We are interested in the quantities $\Lambda_{i,\text{RA}}^{\alpha}(0)$. We can apply the usual standard procedures for the analytical continuation⁸ to each element on the right side of Eqs. (30)–(32), and we get, for instance,

$$\begin{aligned} \Lambda_{x,\text{RA}}^{\alpha}(0) &= \delta_{\alpha,0} + \frac{\pi N(\mu)}{2} \int d\Omega \alpha^2 F_{\alpha}(\Omega) [n(\beta\Omega) + f(\beta\Omega)] \\ &\quad \times \left[\sum_{j,\beta} c_j^{\beta} \frac{\Lambda_{j,\text{RA}}^{\beta+\alpha}(\Omega)}{\Gamma_{\text{qp}}(\Omega)} \right]. \end{aligned} \quad (33)$$

Similar expressions hold true for $\Lambda_{l,\text{RA}}^{\alpha}(0)$ and $\Lambda_{y,\text{RA}}^{\alpha}(0)$.

The quantities $\Lambda_{j,\text{RA}}^{\beta}(\Omega)$ and $\Gamma_{\text{qp}}(\Omega)$ on the right side of Eq. (33) have a significant Ω variation over an electronic

range of energies, whereas the Eliashberg function $\alpha^2 F_\alpha(\Omega)$ limits the energy integration up to the phonon scale ω_{\max} . In this energy range we can then approximate in the integral of Eq. (33), $\Lambda_{j,RA}^\beta(\Omega) \simeq \Lambda_{j,RA}^\beta(0)$, and $\Gamma_{qp}(\Omega) \simeq \Gamma_{qp}(0) = \Gamma_{qp}$, and we obtain a simple set of *algebraic* relations for the vertex function at zero frequency,

$$\Lambda_{x,RA}^\alpha(0) = \delta_{\alpha,0} + \frac{K_\alpha}{\Gamma_{qp}} \sum_{j,\beta} c_j^\beta \Lambda_{j,RA}^{\beta+\alpha}(0),$$

$$\Lambda_{I,RA}^\alpha(0) = \frac{K_\alpha}{\Gamma_{qp}} \sum_{j,\beta} d_j^\beta \Lambda_{j,RA}^{\beta+\alpha}(0),$$

$$\Lambda_{y,RA}^\alpha(0) = \frac{K_\alpha}{\Gamma_{qp}} \sum_{j,\beta} f_j^\beta \Lambda_{j,RA}^{\beta+\alpha}(0).$$

Despite its apparent complexity, such a system of equations admits a simple solution. In particular, by exploiting the symmetric/antisymmetric properties for $\alpha \rightarrow -\alpha$ of the x , I , and y components, respectively, one can see that only three independent components are not zero, i.e., $\Lambda_{x,RA}^0$, $\Lambda_{x,RA}^2$, and $\Lambda_{I,RA}^1$, with the relations, $\Lambda_{x,RA}^2 = \Lambda_{x,RA}^{-2} = i\Lambda_{y,RA}^{-2} = -i\Lambda_{y,RA}^2$ and $\Lambda_{I,RA}^1 = \Lambda_{I,RA}^{-1}$. The system can be further simplified by noting that it can be rewritten in terms of a single self-consistent equation for $\Lambda_{RA}^{\text{tot}}$:

$$\Lambda_{RA}^{\text{tot}} = 1 + \frac{K_0 + 2K_1 + K_2}{\Gamma_{qp}} \Lambda_{RA}^{\text{tot}},$$

whose solution gives

$$\Lambda_{RA}^{\text{tot}}(0) = \frac{\Gamma_{qp}}{\Gamma_{qp} - K_0 - 2K_1 - K_2}. \quad (34)$$

Finally, by expressing the quasiparticle scattering rate Γ_{qp} as a function of the K_α terms as in Eq. (17) we obtain

$$\Gamma_{tr} = K_0 - K_2. \quad (35)$$

Equations (34) and (35) are the main results of the present paper. Their physical insight appears clearly if we express the transport scattering rate in terms of the microscopic electron-phonon interaction, in analogy with result (19) for the quasiparticle scattering rate:

$$\begin{aligned} \Gamma_{tr} = K_0 - K_2 &= \pi N(\mu) \int \frac{d\theta}{2\pi} g_\theta^2 \frac{1 - \cos 2\theta}{2} [n(\beta\omega_\theta) + f(\beta\omega_\theta)] \\ &= \pi N(\mu) \int \frac{d\theta}{2\pi} g_\theta^2 (1 - \cos \theta)(1 + \cos \theta) \\ &\quad \times [n(\beta\omega_\theta) + f(\beta\omega_\theta)]. \end{aligned} \quad (36)$$

Taking into account the expression of the quasiparticle scattering rate Γ_{qp} in Eq. (19), we can write Eq. (36) as

$$\langle \Gamma_{tr} \rangle_\theta = \langle \Gamma_{qp} (1 - \cos \theta) \rangle_\theta. \quad (37)$$

This analysis shows thus that a fully quantum derivation of the dc conductivity yields in doped graphene the same result than the standard Boltzmann theory. In particular we can see that, although the vertex function is \mathbf{k} independent in

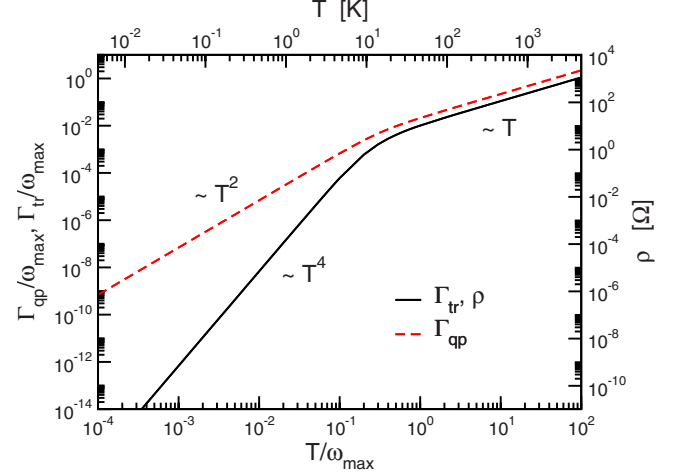


FIG. 6. (Color online) Temperature behavior of the quasiparticle scattering rate Γ_{qp} and of the transport scattering rate Γ_{tr} for $\mu = 0.1$ eV, corresponding to $\omega_{\max} \approx 4$ meV. The transport scattering rate Γ_{tr} can be also expressed as a function of resistivity, $\rho = 4VT_{tr}/N_K N_s \hbar e^2 v_F^2 N(\mu)$, as plotted on the right-side scale.

graphene, the effect of current vertex corrections is to add, just as in common systems, the additional angular factor $1 - \cos \theta$ in the phase space probed by the electron-phonon interaction, giving rise to a suppression of the *forward* scattering. The effects of such angular factor can be remarkably traced in the temperature dependence of the transport scattering rate $\Gamma_{tr} = K_0 - K_2$ (and hence of the resistivity $\rho = 1/\sigma$) compared with the quasiparticle one $\Gamma_{qp} = 2(K_0 + K_1)$. An analytical derivation of the K_α coefficients is reported in Appendix A and the corresponding temperature dependence of Γ_{tr} and Γ_{qp} is shown in Fig. 6. These results are pretty well consistent with the standard Boltzmann theory.^{18,19} In the high-temperature limit $T \gg \omega_{\max}$ only the K_0 component survives, with $K_0 = \pi N(\mu) IT / 2\hbar v_s$ (see Appendix A), so that $\Gamma_{tr}, \Gamma_{qp} \sim T$. On the other hand in the Bloch-Grüneisen regime, just as in common metals, we recover the usual $\Gamma_{tr} \sim T^4$, while $\Gamma_{qp} \sim T^2$. This different dependence can be understood by noting that the low-temperature behavior of Γ_{qp} in Eq. (17) is dominated by the leading order $\sim T^2$ of K_0 and K_1 , whereas the leading orders K_0 and K_2 in Eq. (35) cancel out so that the temperature behavior of Γ_{tr} in this regime stems from the higher-order $\sim T^4$ contributions.

V. BREAKING THE CHIRALITY

In Sec. IV we have evaluated the dc conductivity in chiral doped graphene by using a quantum approach based on the Kubo formula. We have shown that, although the vertex function is momentum independent, the Boltzmann results are fully reproduced, even for what concerns the presence of the so-called angular transport factor $1 - \cos \theta$ which suppresses forward scattering. We would like to stress however that the resulting validity of the Boltzmann theory is by no means trivial. Indeed, as we have shown, the robustness of the Boltzmann results is due to the chiral structure itself of graphene, $\hat{H}_{\mathbf{k}} = \hbar v_F \mathbf{k} \cdot \boldsymbol{\sigma}$, which translates in the direction of

the Pauli matrix pseudospin $\boldsymbol{\sigma}$ the role which in common metals is played by the momentum \mathbf{k} direction.

Such observation raises the question about the validity of the Boltzmann result when the chiral structure of graphene is affected by external fields. This happens, for instance, in the presence of a weak sublattice inequivalence, where an energy potential difference between the two sublattices, besides opening a gap at the Dirac point,^{34,43} gives rise also to a mixing of the chiral eigenstates and to a loss of chirality close to the Dirac point. Such reduced role of the chirality close to the Dirac point has been traced, for instance, in Refs. 29 and 30 in the intensity profile along the constant-energy contours probed by angle-resolved photoemission.^{29,30} The validity of the Boltzmann results even in this context needs thus to be revised.

To this aim in this section we consider doped graphene in the presence of a weak inequivalence between the two carbon sublattices, parametrized in terms of a different sublattice potential Δ :

$$\hat{H}_{\mathbf{k}} = \hbar v_F \mathbf{k} \cdot \boldsymbol{\sigma} + \Delta \hat{\sigma}_z, \quad (38)$$

The energy spectrum is easily obtained from Eq. (38), $E_{\mathbf{k}} = \sqrt{(\hbar v_F k)^2 + \Delta^2}$, showing the opening of a gap at the Dirac point.

Let us consider for the moment the case of a noninteracting system. The presence of Δ induces an explicit $\propto \hat{\sigma}_z$ component in both the Green's function and self-energy. Equation (6) is thus generalized as $\hat{G}(\mathbf{k}, n) = \sum_{i=x,y,z} G_i(\mathbf{k}, n) \hat{\sigma}_i$, where $G_x(\mathbf{k}, n) = G_+(E, n)$, $G_y(\mathbf{k}, n) = \gamma_{\text{off}}(E) G_-(E, n) \cos \phi$, $G_z(\mathbf{k}, n) = \gamma_z(E) G_-(E, n) \sin \phi$, and $G_+(E, n) = \frac{1}{2} \left[\frac{1}{i\hbar\omega_n + \mu - E} \pm \frac{1}{i\hbar\omega_n + \mu + E} \right]$, with

$$G_{\pm}(E, n) = \frac{1}{2} \left[\frac{1}{i\hbar\omega_n + \mu - E} \pm \frac{1}{i\hbar\omega_n + \mu + E} \right],$$

$\gamma_{\text{off}}(E) = \epsilon/E$, and $\gamma_z(E) = \Delta/E$. Here we denote $\epsilon = \hbar v_F k$ and $E = \sqrt{\epsilon^2 + \Delta^2}$.

Since we are interested in the doped graphene, where $|\mu| \gg \omega_{\text{max}}$, and we assume $\mu > 0$, we can as usual consider only the upper band, and we can restrict the electronic states on the Fermi surface, for which $E \approx \mu$ and $\epsilon \approx \sqrt{1 - \Delta^2/\mu^2}$, and we have

$$G_i(E, n) = \frac{\gamma_i}{2} g(E, n), \quad (39)$$

where $\gamma_x = 1$, $\gamma_y = \gamma_z = \gamma_{\text{off}} = \sqrt{1 - \Delta^2/\mu^2}$, and $\gamma_z = \Delta/\mu$ and where $g(E, n) = 1/(i\hbar\omega_n + \mu - E)$.

Plugging Eq. (39) into Eq. (7), we can write

$$\Sigma_i(n) = \frac{T}{2} \sum_m W(n-m) g_{\text{loc}}(m),$$

$$\Sigma_{\text{off}}(n) = \frac{\gamma_{\text{off}} T}{2} \sum_m W_1(n-m) g_{\text{loc}}(m),$$

$$\Sigma_z(n) = \frac{\gamma_z T}{2} \sum_m W(n-m) g_{\text{loc}}(m),$$

where $g_{\text{loc}}(m) = N(\mu) \int dE g(E, m)$. After the standard analytical continuation on the real axis, we can see as usual that the real part of self-energy vanishes and the imaginary parts of the different components give rise to the corresponding scattering rates

$$\Gamma_I = 2K_0, \quad (40)$$

$$\Gamma_{\text{off}} = \gamma_{\text{off}} 2K_1, \quad (41)$$

$$\Gamma_z = \gamma_z 2K_0. \quad (42)$$

Inserting these relations in the matrix expression for the Green's function, after some careful derivation described in Appendix B, we can write a Green's function in the presence of interaction in the form of Eq. (18), with

$$\begin{aligned} \Gamma_{\text{qp}} &= \Gamma_I + \gamma_{\text{off}} \Gamma_{\text{off}} + \gamma_z \Gamma_z = (1 + \gamma_z^2) 2K_0 + \gamma_{\text{off}}^2 2K_1 \\ &= \left(1 + \frac{\Delta^2}{\mu^2}\right) 2K_0 + \left(1 - \frac{\Delta^2}{\mu^2}\right) 2K_1. \end{aligned}$$

We can write thus

$$\begin{aligned} \Gamma_{\text{qp}} &= \pi N(\mu) \int \frac{d\theta}{2\pi} g_{\theta}^2 [n(\beta\omega_{\theta}) + f(\beta\omega_{\theta})] \\ &\quad \times \left[\left(1 + \frac{\Delta^2}{\mu^2}\right) + \left(1 - \frac{\Delta^2}{\mu^2}\right) \cos \theta \right]. \end{aligned} \quad (43)$$

Equation (43) shows in a direct way the reduced effect of the chirality on the quasiparticle scattering rate in the presence of a sublattice inequivalence. For instance, we can see that the backscattering $\theta = \pi$ is now not completely suppressed but it is reduced by a factor of Δ^2/μ^2 with respect to the forward scattering $\theta = 0$. For $|\mu| = \Delta$, when the chemical potential is on the edge of the gap,²⁹ the K_1 angular dependence disappears completely and the quasiparticle scattering is completely isotropic with no effect of chirality.

Let us consider now the dc conductivity. Using the same derivation as in Sec. IV, we can still write a set of equations as Eqs. (30)–(32) with the same c_i^α , d_i^α , and f_i^α and rescaled quantities $K_0 \rightarrow \gamma_{\text{off}}^2 K_0$, $K_1 \rightarrow (1 + \gamma_z^2) K_1$, and $K_2 \rightarrow \gamma_{\text{off}}^2 K_2$. The presence of $\propto \hat{\sigma}_z$ terms in the Green's function gives rise in addition to a finite z component Λ_z^α . After lengthy but straightforward calculations we can still write the same self-consistent equation for the total vertex function as before, with the rescaling of the K_α coefficients discussed above. The final result is

$$\Lambda_{\text{RA}}^{\text{tot}}(0) = \frac{\gamma_{\text{off}}^2 \Gamma_{\text{qp}}}{\Gamma_{\text{qp}} - \gamma_{\text{off}}^2 K_0 - 2(1 + \gamma_z^2) K_1 - \gamma_{\text{off}}^2 K_2},$$

so that

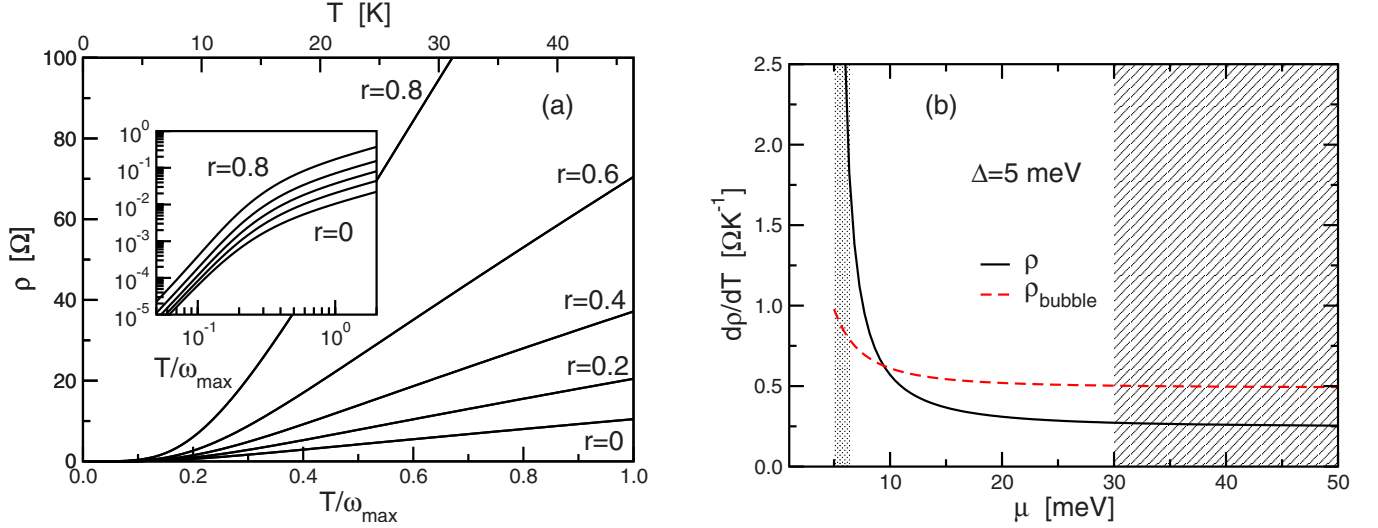


FIG. 7. (Color online) (a) Temperature dependence of the resistivity for different dopings in the presence of a weak sublattice inequivalence, giving rise to the gap Δ . Here $r = \Delta^2/\mu^2$. Resistivity has been computed using the transport scattering time in Eq. (44). Inset: same quantities on a log-log scale. (b) Doping dependence of the high-temperature slope of the resistivity in graphene in the presence of a gap ($\Delta = 5$ meV). The dashed (red) line is result (47) obtained with the bare bubble, while the solid (black) line represents resistivity (46) computed with full inclusion of vertex corrections. The shaded area at $\mu > 30$ meV represents the range of dopings investigated in Ref. 28, while in the gray area around 5 meV the validity of Eq. (46) fails because $|\mu| - \Delta \leq \Gamma_{qp}$ ($\Gamma_{qp} = 1.4$ meV has been computed here for $T = 300$ K).

$$\begin{aligned} \Gamma_{tr} &= \frac{\Gamma_{qp} - \gamma_{off}^2 K_0 - 2(1 + \gamma_z^2) K_1 - \gamma_{off}^2 K_2}{\gamma_{off}^2} \\ &= \frac{\mu^2 + 3\Delta^2}{\mu^2 - \Delta^2} K_0 - \frac{4\Delta^2}{\mu^2 - \Delta^2} K_1 - K_2. \end{aligned} \quad (44)$$

Equation (44) looks at first sight quite dim. However, taking into account the explicit angular dependence of the Eliashberg functions $\alpha^2 F_\alpha$ and of the coefficients K_α , we can rearrange Eq. (44) in the form

$$\langle \Gamma_{tr} \rangle_\theta = \left(1 - \frac{\Delta^2}{\mu^2}\right)^{-1} \langle \Gamma_{qp}(1 - \cos \theta) \rangle_\theta, \quad (45)$$

where the presence of the angular term $(1 - \cos \theta)$ suggests again the validity of the Boltzmann result even in this case where the chirality of graphene close to the Dirac point is affected by the sublattice inequivalence. As far as the prefactor is concerned, one could in principle justify this as well within the Boltzmann framework by taking into account that the opening of the gap affects also the Fermi velocity of the eigenstates of Hamiltonian (38). Thus, following the Boltzmann prescription, the velocity in the basis of the eigenstates is $v_k = \hbar^{-1} d\sqrt{(\hbar v_F k)^2 + \Delta^2}/dk = v_F \epsilon_k / \sqrt{\epsilon_k^2 + \Delta^2} \approx v_F \sqrt{1 - \Delta^2/\mu^2}$, where $\epsilon_k = \hbar v_F k$ and $\sqrt{\epsilon_k^2 + \Delta^2} \approx \mu$ at the Fermi level. Thus, the additional $(1 - \Delta^2/\mu^2)$ factor, which we obtained in Eq. (45) associated with vertex corrections, will appear in the Boltzmann expression for the conductivity $\sigma_B = e^2 N(\mu) v^2 / 2 \langle \Gamma_B \rangle$ associated to the v^2 term instead of the scattering rate, which is simply $\langle \Gamma_B \rangle_\theta = \langle \Gamma_{qp}(1 - \cos \theta) \rangle_\theta$.

VI. DISCUSSION

In Secs. IV and V we have shown that, in the limit where the chemical potential is the largest energy scale of the system, the Boltzmann theory is still valid for graphene even in the presence of a weak sublattice inequivalence which gives rise to a gap Δ . A possible outcome of these calculations beyond this ‘‘Boltzmann regime’’ is suggested by the observation of the (weak) doping dependence of the resistivity ρ that follows from Eq. (45). As shown in Fig. 7(a), both the low-temperature ($T \ll \omega_{max}$) and the high-temperature ($T \gg \omega_{max}$) regimes acquire a doping dependence, here parametrized in terms of the ratio $r = (\Delta/\mu)^2$. Particularly interesting appears the high-temperature regime where, using Eqs. (44) and (A4), one finds

$$\rho = \frac{\mu^2 + 3\Delta^2}{\mu^2 - \Delta^2} \frac{\pi D^2}{4\hbar e^2 v_F^2 v_s^2 \rho_m} T, \quad (46)$$

which implies a *significant* increase in the linear slope as one approaches the Dirac point $\mu \rightarrow \Delta$, as shown in Fig. 7(b). Observe that if one would use instead the single-bubble result for the dc conductivity, the resistivity would be proportional to the quasiparticle scattering rate Γ_{qp} , so that according to Eq. (43) one would obtain

$$\rho_{bare} = \left(1 + \frac{\Delta^2}{\mu^2}\right) \frac{\pi D^2}{4\hbar e^2 v_F^2 v_s^2 \rho_m} T, \quad (47)$$

which has a much weaker doping dependence, as shown in Fig. 7(b). Remarkably, an increase in the linear slope as μ decreases has been observed in recent measurements of resistivity in doped graphene samples.^{27,28} Indeed, while the measured crossover from a power-law behavior to a linear- T behavior points toward the electron-phonon scattering as the

source of the temperature dependence, the fact that the slope of the linear term decreases as doping increases, and eventually saturates at enough large doping, is unexplained within existing theories. Equation (46) could suggest a possible mechanism for this doping dependence, even though in the regime of validity of this equation the quantitative variations in the slope are expected to be much smaller than what were experimentally measured. Indeed, recent tunneling experiments performed in a similar suspended graphene sample have found a gap at the Dirac point $\Delta \approx 5$ meV.⁴⁴ This small value of the gap, compared to the relevant values $\mu \approx 30\text{--}70$ meV of the chemical potential in the samples investigated in Ref. 28, would lead, in Eq. (46), to a variation in the slope of only few percent, as shown in Fig. 7(b). However, one should keep in mind that Eq. (46) has been derived in the limit $\Gamma_{\text{qp}} \ll \mu$. Thus, only the full solution in the crossover region where the Dirac point is approached can discriminate if the doping dependence reported in Refs. 27 and 28 is an effect of a small gap opening which goes beyond the Boltzmann approach. Analogously, it can be worthy also to investigate alternative scenarios⁴⁵ for the gap opening that have been suggested by photoemission results in epitaxial graphene,^{46,47} where the gap $\Delta \approx 100$ meV is comparable to the chemical potential in the interesting doping regime.

VII. CONCLUSIONS

In summary, in this paper we outlined the issue of the calculation of the current vertex corrections for electron-phonon scattering in graphene within the Kubo formalism. While previous works investigated the role of vertex corrections in the presence of impurity scattering,^{24,26} here we address the issue of vertex corrections in graphene when the scattering mechanism arises from electron-phonon interactions, which have a nontrivial momentum dependence. We analyzed in particular the case of doped graphene, when μ is the largest energy scale of the system (i.e., $|\mu| \gg \omega_{\text{max}}, \Gamma_{\text{qp}}$). In this regime the calculations can be performed explicitly, leading to an analytical derivation of the transport scattering rate which appears in the dc conductivity. Remarkably, we found that despite the lack of direction dependence of the quasiparticle velocity in graphene, the matrix structure associated to the current vertex plays a similar role as the momentum dependence of the renormalized vertex in ordinary metals, leading to a confirmation of the Boltzmann approach. Such a result is confirmed also in the presence of a sublattice inequivalence, which leads to a gapped Dirac spectrum and introduces a doping dependence of the resistivity that can be a promising candidate to explain existing experimental data in doped graphene samples. With respect to the formalism based on the quantum kinetic equations,^{20,22} which is also aimed at investigating the applicability of the Boltzmann result, the present approach based on the calculation of vertex corrections for the conductivity bubble has the main advantage of being suitable of a direct extension at finite frequency. Such an extension will lead to a full quantum treatment of the conductivity in graphene, and will be the subject of a future work.

ACKNOWLEDGMENT

We acknowledge financial support from MIUR under the research program MIUR-PRIN 2007.

APPENDIX A: HARMONIC COMPONENTS OF THE ELIASHBERG FUNCTIONS AND K_α COEFFICIENTS

In this appendix we provide an explicit expression for the harmonic components of Eliashberg functions $\alpha^2 F_\alpha(\Omega)$, and we calculate the temperature dependence of the corresponding functions $K_\alpha(T)$. We recall the definition of the momentum-dependent Eliashberg function,

$$\alpha^2 F(\mathbf{k} - \mathbf{k}', \Omega) = |g_{\mathbf{k}-\mathbf{k}'}|^2 \delta(\Omega - \omega_{\mathbf{k}-\mathbf{k}'}),$$

where $\omega_{\mathbf{q}} \approx \hbar v_s |\mathbf{q}|$. Following Ref. 19, we notice that $|g_{\mathbf{q}}|^2 \propto |\mathbf{q}|$, so that we can write $|g_{\mathbf{q}}|^2 = I |\mathbf{q}|$, where $I = \hbar D^2 / 2V \rho_m v_s$, D is the deformation potential, V is the volume of the two-dimensional unit cell, and ρ_m is the graphene mass density. Typical values are $D \approx 19$ eV, $\rho_m = 7.6 \times 10^{-8}$ g/cm², $v_s = 2 \times 10^6$ cm/s, and $v_F = 10^6$ m/s. Restricting the electron momenta on the Fermi surface, $|\mathbf{k}| \approx |\mathbf{k}'| \approx k_F$, we can write $|\mathbf{q}| = 2k_F \sin[(\phi - \phi')/2]$, and the Eliashberg function will result to depend only on the exchanged angle $\theta = \phi - \phi'$:

$$\alpha^2 F(\theta, \Omega) = 2Ik_F \sin(\theta/2) \delta[\Omega - \omega_{\text{max}} \sin(\theta/2)], \quad (\text{A1})$$

where we recall that $\omega_{\text{max}} = 2\hbar v_s k_F$.

The angular components $\alpha^2 F_\alpha$ will be evaluated simply projecting Eliashberg function (A1) on the spherical harmonics $\psi_\alpha(\phi) = e^{i\alpha\phi}$. We have thus

$$\begin{aligned} \alpha^2 F_\alpha(\Omega) &= 2Ik_F \int_0^{2\pi} \frac{d\theta}{2\pi} \sin(\theta/2) e^{i\alpha\theta} \delta[\Omega - \omega_{\text{max}} \sin(\theta/2)] \\ &= 2Ik_F \int_0^\pi \frac{d\theta}{\pi} \sin \theta e^{i2\alpha\theta} \delta[\Omega - \omega_{\text{max}} \sin \theta]. \end{aligned}$$

The δ function has two solutions for $\theta \in [0; \pi]$, one for $\theta = y_\Omega$ and one for $\theta = \pi - y_\Omega$, where $y_\Omega = \arcsin(\Omega / \omega_{\text{max}})$. We can write thus

$$\begin{aligned} \alpha^2 F_\alpha(\Omega) &= 2Ik_F \int_0^\pi \frac{d\theta}{\pi} \sin \theta e^{i2\alpha\theta} \frac{1}{|\omega_{\text{max}} \cos(\theta)|} \\ &\quad \times [\delta(\theta - y_\Omega) + \delta(\theta - \pi + y_\Omega)] \\ &= \frac{4Ik_F}{\pi \omega_{\text{max}}^2} \frac{\Omega \theta (\omega_{\text{max}} - \Omega)}{\sqrt{1 - (\Omega / \omega_{\text{max}})^2}} \frac{1}{2} [e^{i2\alpha y_\Omega} + e^{i2\alpha(\pi - y_\Omega)}] \\ &= \frac{2I}{\pi \hbar v_s} \frac{\Omega \cos(2\alpha y_\Omega) \theta (\omega_{\text{max}} - \Omega)}{\sqrt{\omega_{\text{max}}^2 - \Omega^2}}, \quad (\text{A2}) \end{aligned}$$

where we made use of $\sin(y_\Omega) = \sin(\pi - y_\Omega) = \Omega / \omega_{\text{max}}$ and $|\cos(y_\Omega)| = |\cos(\pi - y_\Omega)| = \sqrt{1 - (\Omega / \omega_{\text{max}})^2}$.

Inserting Eq. (A2) into Eq. (16) which defines the K_α function, we can obtain their temperature dependence. By rescaling the integration variable to $y = \beta\Omega$, we have

$$K_\alpha = \frac{N(\mu)I}{\hbar v_s} \frac{T^2}{\omega_{\max}} \int_0^{\beta\omega_{\max}} dy \frac{y}{\sqrt{1 - (y/\beta\omega_{\max})^2}} \times \cos\left(2\alpha \arcsin \frac{y}{\beta\omega_{\max}}\right) [n(y) + f(y)]. \quad (\text{A3})$$

In the low-temperature limit $T \ll \omega_{\max}$ we can retain the leading terms in powers of $y/\beta\omega_{\max}$ in the integrand and send the upper limit of integration to infinity, $\beta\omega_{\max} \rightarrow \infty$. We obtain thus

$$K_\alpha = \frac{N(\mu)I}{\hbar v_s} \frac{T^2}{\omega_{\max}} \left[a_1 + a_3 \frac{1 - 4\alpha^2}{2} \frac{T^2}{\omega_{\max}^2} \right],$$

where $a_n = \int_0^\infty dy y^n [n(y) + f(y)]$, and in particular, $a_1 = \pi^2/4$ and $a_3 = \pi^4/8$. In the opposite high-temperature limit $T \gg \omega_{\max}$, we can instead compute the integrand function in Eq. (A3) as $y \rightarrow 0$. In this case, due to the rapid oscillations of the cosine term, all the harmonics vanish except the $\alpha = 0$ one, which displays a linear- T dependence:

$$K_0(T) = \frac{\pi N(\mu)I}{2\hbar v_s} T. \quad (\text{A4})$$

APPENDIX B: TOTAL QUASIPARTICLE SCATTERING RATE IN THE PRESENCE OF SUBLATTICE INEQUVALENCE

In this appendix we derive the effective total quasiparticle scattering rate in graphene in the presence of sublattice inequivalence. Let us start from the scattering rates in Eqs. (40)–(42), which we can write in the matricial form:

$$\hat{\Gamma} = \Gamma_I \hat{I} + \Gamma_{\text{off}} [\cos \phi \hat{\sigma}_x + \sin \phi \hat{\sigma}_y] + \Gamma_z \hat{\sigma}_z. \quad (\text{B1})$$

Considering the Hamiltonian in Eq. (38), we have then

$$\hat{G}^{-1}(\epsilon, \omega) = (\hbar\omega + i\Gamma_I) \hat{I} + (\Delta - i\Gamma_z) \hat{\sigma}_z - (\epsilon - i\Gamma_{\text{off}}) [\cos \phi \hat{\sigma}_x + \sin \phi \hat{\sigma}_y].$$

The spectral function, whose width determines the total ef-

fective quasiparticle scattering rate, is associated with the G_I term, which results to

$$G_I(\epsilon, \omega) = \frac{\hbar\omega + \mu + i\Gamma_I}{(\hbar\omega + \mu + i\Gamma_I)^2 - (\epsilon - i\Gamma_{\text{off}})^2 - (\Delta - i\Gamma_z)^2}. \quad (\text{B2})$$

In order to identify the total effective quasiparticle scattering rate, we expand now the denominator and write, in particular,

$$\begin{aligned} & (\epsilon - i\Gamma_{\text{off}})^2 + (\Delta - i\Gamma_z)^2 \\ &= \epsilon^2 + \Delta^2 - \Gamma_{\text{off}}^2 - \Gamma_z^2 - 2i(\epsilon\Gamma_{\text{off}} + \Delta\Gamma_z). \end{aligned}$$

Since $\epsilon^2 + \Delta^2 \approx \mu$ and $\Gamma_{\text{off}}, \Gamma_z \ll |\mu|$, we can neglect $\Gamma_{\text{off}}^2 - \Gamma_z^2$ with respect to $E^2 = \epsilon^2 + \Delta^2$ and, at the same order, we can write

$$\begin{aligned} E^2 - 2i(\epsilon\Gamma_{\text{off}} + \Delta\Gamma_z) &\approx \left[E - i \left(\frac{\epsilon}{E} \Gamma_{\text{off}} + \frac{\Delta}{E} \Gamma_z \right) \right]^2 \\ &\approx \left[E - i \left(\sqrt{1 - \frac{\Delta^2}{\mu^2}} \Gamma_{\text{off}} + \frac{\Delta}{\mu} \Gamma_z \right) \right]^2. \end{aligned}$$

Plugging this result into Eq. (B2), we can now split the resulting Green's function into the usual two contributions from the upper and lower bands,

$$G_I(E, \omega) = \frac{1}{2} \sum_{s=\pm} \frac{1}{\hbar\omega + \mu + i\Gamma_I \mp E \pm i\Gamma_\pm},$$

with

$$\Gamma_\pm = \Gamma_I \pm \left(\sqrt{1 - \frac{\Delta^2}{\mu^2}} \Gamma_{\text{off}} + \frac{\Delta}{\mu} \Gamma_z \right),$$

so that at the Fermi level in the upper band we obtain

$$\Gamma_{\text{qp}} = \Gamma_I + \sqrt{1 - \frac{\Delta^2}{\mu^2}} \Gamma_{\text{off}} + \frac{\Delta}{\mu} \Gamma_z.$$

¹A. H. Castro Neto, F. Guinea, N. M. R. Peres, K. S. Novoselov, and A. K. Geim, arXiv:0709.1163, Rev. Mod. Phys. (to be published).
²T. Ando and T. Nakanishi, J. Phys. Soc. Jpn. **67**, 1704 (1998).
³P. A. Lee, Phys. Rev. Lett. **71**, 1887 (1993).
⁴P. J. Hirschfeld, W. O. Putikka, and D. J. Scalapino, Phys. Rev. B **50**, 10250 (1994).
⁵Y. S. Lee, K. Segawa, Z. Q. Li, W. J. Padilla, M. Dumm, S. V. Dordevic, C. C. Homes, Y. Ando, and D. N. Basov, Phys. Rev. B **72**, 054529 (2005).
⁶E. McCann and V. I. Fal'ko, Phys. Rev. Lett. **96**, 086805 (2006).
⁷T. Holstein, Ann. Phys. (N.Y.) **29**, 410 (1964).
⁸G. D. Mahan, *Many-Particle Physics* (Plenum, New York, 1981).
⁹K. Nomura and A. H. MacDonald, Phys. Rev. Lett. **96**, 256602 (2006).

¹⁰T. Ando, J. Phys. Soc. Jpn. **75**, 074716 (2006).
¹¹E. H. Hwang, S. Adam, and S. Das Sarma, Phys. Rev. Lett. **98**, 186806 (2007).
¹²S. Adam, E. H. Hwang, V. Galitski, and S. Das Sarma, Proc. Natl. Acad. Sci. U.S.A. **104**, 18392 (2007).
¹³D. S. Novikov, Phys. Rev. B **76**, 245435 (2007).
¹⁴T. Stauber, N. M. R. Peres, and F. Guinea, Phys. Rev. B **76**, 205423 (2007).
¹⁵N. M. R. Peres, J. M. B. Lopes dos Santos, and T. Stauber, Phys. Rev. B **76**, 073412 (2007).
¹⁶S. Adam and S. Das Sarma, Phys. Rev. B **77**, 115436 (2008).
¹⁷S. Adam and S. Das Sarma, Solid State Commun. **146**, 356 (2008).
¹⁸E. H. Hwang and S. Das Sarma, Phys. Rev. B **77**, 195412 (2008).

- ¹⁹E. H. Hwang and S. Das Sarma, *Phys. Rev. B* **77**, 115449 (2008).
- ²⁰M. Auslender and M. I. Katsnelson, *Phys. Rev. B* **76**, 235425 (2007).
- ²¹M. Trushin and J. Schliemann, *Phys. Rev. Lett.* **99**, 216602 (2007).
- ²²M. Trushin and J. Schliemann, *EPL* **83**, 17001 (2008).
- ²³J. M. Ziman and G. D. Mahan, *Electrons and Phonons* (Oxford University Press, New York, 1960).
- ²⁴N. H. Shon and T. Ando, *J. Phys. Soc. Jpn.* **67**, 2421 (1998).
- ²⁵E. McCann, K. Kechedzhi, V. I. Fal'ko, H. Suzuura, T. Ando, and B. L. Altshuler, *Phys. Rev. Lett.* **97**, 146805 (2006).
- ²⁶K. Kechedzhi, O. Kashuba, and V. I. Fal'ko, *Phys. Rev. B* **77**, 193403 (2008).
- ²⁷J. H. Chen, C. Jang, S. Xiao, M. Ishigami, and M. S. Fuhrer, *Nat. Nanotechnol.* **3**, 206 (2008).
- ²⁸K. I. Bolotin, K. J. Sikes, J. Hone, H. L. Stormer, and P. Kim, *Phys. Rev. Lett.* **101**, 096802 (2008).
- ²⁹M. Mucha-Kruczyński, O. Tsypliyat'ev, A. Grishin, E. McCann, V. I. Fal'ko, A. Bostwick, and E. Rotenberg, *Phys. Rev. B* **77**, 195403 (2008).
- ³⁰A. Bostwick, T. Ohta, J. L. McChesney, K. V. Emtsev, T. Seyller, K. Horn, and E. Rotenberg, *New J. Phys.* **9**, 385 (2007).
- ³¹Z. Q. Li, E. A. Henriksen, Z. Jiang, Z. Hao, M. C. Martin, P. Kim, H. L. Stormer, and D. N. Basov, *Nat. Phys.* **4**, 532 (2008).
- ³²A. H. Castro Neto and F. Guinea, *Phys. Rev. B* **75**, 045404 (2007).
- ³³Ge. G. Samsonidze, E. B. Barros, R. Saito, J. Jiang, G. Dresselhaus, and M. S. Dresselhaus, *Phys. Rev. B* **75**, 155420 (2007).
- ³⁴J. L. Mañes, F. Guinea, and M. A. H. Vozmediano, *Phys. Rev. B* **75**, 155424 (2007).
- ³⁵C.-H. Park, F. Giustino, M. L. Cohen, and S. G. Louie, *Phys. Rev. Lett.* **99**, 086804 (2007).
- ³⁶N. Bonini, M. Lazzeri, N. Marzari, and F. Mauri, *Phys. Rev. Lett.* **99**, 176802 (2007).
- ³⁷M. Calandra and F. Mauri, *Phys. Rev. B* **76**, 205411 (2007).
- ³⁸W.-K. Tse and S. Das Sarma, *Phys. Rev. Lett.* **99**, 236802 (2007).
- ³⁹D. M. Basko and I. L. Aleiner, *Phys. Rev. B* **77**, 041409(R) (2008).
- ⁴⁰A. B. Migdal, *Zh. Eksp. Teor. Fiz.* **34**, 1438 (1958) [*Sov. Phys. JETP* **7**, 996 (1958)].
- ⁴¹G. M. Eliashberg, *Zh. Eksp. Teor. Fiz.* **38**, 966 (1960) [*Sov. Phys. JETP* **11**, 696 (1958)].
- ⁴²V. P. Gusynin, S. G. Sharapov, and J. P. Carbotte, *Phys. Rev. Lett.* **96**, 256802 (2006).
- ⁴³V. P. Gusynin, S. G. Sharapov, and J. P. Carbotte, *Int. J. Mod. Phys. B* **21**, 4611 (2007).
- ⁴⁴G. Li, A. Luican, and E. Y. Andrei, arXiv:0803.4016 (unpublished).
- ⁴⁵L. Benfatto and E. Cappelluti, *Phys. Rev. B* **78**, 115434 (2008).
- ⁴⁶S. Y. Zhou, G.-H. Gweon, A. V. Fedorov, P. N. First, W. A. de Heer, D.-H. Lee, F. Guinea, A. H. Castro Neto, and A. Lanzara, *Nature Mater.* **6**, 770 (2007).
- ⁴⁷S. Y. Zhou, D. A. Siegel, A. V. Fedorov, and A. Lanzara, *Physica E (Amsterdam)* **40**, 2642 (2008).